G-Quadruplex DNA

DOI: 10.1002/anie.201307594

Reversible Stabilization of Transition-Metal-Binding DNA G-Quadruplexes**

*David M. Engelhard, Roberta Pievo, and Guido H. Clever**

For the biological function of oligonucleotides, not only the primary sequence but also the precise secondary and tertiary structure is essential, especially in the context of protein interactions. DNA is known to form a number of secondary structures beyond the double helix such as triplexes, the four-stranded i-motif, and G-quadruplexes.[1] The latter result from the self-assembly of guanine-rich oligonucleotides by Hoogsteen base pairing, thus forming stacked guanine tetrads stabilized by central cations. G-quadruplexes have gained increasing attention,[2,3] as studies indicate that their in vivo formation both prevents human telomere elongation, and therefore shortens cancer cell lifetimes, and also plays a role in the gene expression of oncogenes.[4]

Although the G-quartets themselves show little structural diversity (*syn*/*anti* conformation of guanosine), complexity is introduced by the relative strand orientation (parallel/anti-parallel) and variations in the topology and sequence of single-stranded loops.[5] Biomimetic G-quadruplexes with an increased and switchable stability as well as diagnostically exploitable properties such as fluorescence[6] and magnetism may be useful for the labeling and capturing of specific binders from a biological matrix.[7] It is thus of great interest to design discrete G-quadruplex probes which allow for control over the de- and rehybridization thermodynamics and kinetics, the choice of loop sequence and topology, and the introduction of nonbiogenic functionalities by automated DNA synthesis.[8] In addition, the selective formation of such functionalized, bioartificial G-quadruplex constructs may prove valuable in the emerging field of DNA nanotechnology.[9,10]

Up until now studies concerned with the stabilization and labeling of G-quadruplexes focused mainly on the binding of planar organic compounds and flat metal complexes through noncovalent interactions such as end-on π-stacking and intercalation.[2c,11] In recent years, however, the concept of metal–base pairing has demonstrated that the synthetic exchange of the natural nucleobases for ligands allows for the incorporation of transition metals inside duplex DNA.[12,13] Both the higher stability of the metal–ligand bonding (as compared to the H-bonding in Watson–Crick base pairs) and the unique magnetic and electronic properties of the incorporated metals have led to a number of functional nanodevices. Examples include a system capable of a reversible hairpin–duplex transformation,[14] Ag/Hg-selective multiplex sensors,[15] ferro- and antiferromagnetically coupled linear arrays,[16] programmable mixed-metal stacks,[17] and metal-controlled single-molecule conductors.[18]

All of these functional systems, however, are based on double-stranded DNA. With respect to other DNA secondary structures, only a small number of metal-binding architectures such as triplexes[19,13a] and three-way junctions[20] have been reported.[21] In particular, only very few examples of G-quadruplexes carrying covalently bound metal complexes have been reported including the binding of mercury to thymine bases in the loops of a bimolecular G-quadruplex,[22] the cleavage of human telomeric sequences by a covalently attached chelate–cerium(IV) complex,[23] and a bimolecular G-quadruplex with bipyridine units in the loops.[24]

Here, we report the first tetramolecular G-quadruplex terminated by a "metal–base tetrad", in which each of the guanosines in one guanine-tetrad motif is formally replaced by a monodentate pyridine ligand. Together the four pyridine units coordinate to a transition metal ion such as Cu^{II} or Ni^{II} in a square-planar fashion, thus significantly stabilizing the whole assembly towards thermal denaturation. The reversibility of the metal-triggered quadruplex stabilization as monitored by melting temperature studies, circular dichroism (CD), and gel electrophoresis is presented. Additionally, electron paramagnetic resonance (EPR) spectroscopic evidence for the nature of the metal coordination is given.[16a,b]

The oligonucleotides reported in this work contain a guanine sequence ($n = 3$–5), which is necessary for the quadruplex formation, and a pyridyl donor functionality attached to the 5′-end of the strand by means of a propane-1,3-diyl linker. This linker length was chosen based on a molecular modeling study (see Figure 1c and the Supporting Information). The synthesis commences with the attachment of the linker to 4-chloropyridine hydrochloride (**1**). Subsequent phosphorylation leads to phosphoramidite **2**, which is then used in the automated solid-state oligonucleotide synthesis yielding the single strands $\mathbf{L^1}d(G_n)$ (Figure 1a, see the Supporting Information for experimental details).

As with unmodified G-quadruplexes, the formation of $[\mathbf{L^1}d(G_n)]_4$ requires a high electrolyte concentration and low temperatures (Figure 1b).[25] The annealing process is slow

[*] D. M. Engelhard, Prof. Dr. G. H. Clever
Institute of Inorganic Chemistry
Georg-August University Göttingen
Tammannstrasse 4, 37077 Göttingen (Germany)
E-mail: gclever@gwdg.de
Homepage: http://www.clever-lab.de
Dr. R. Pievo
Max Planck Institute for Biophysical Chemistry
Am Fassberg 11, 37077 Göttingen (Germany)

[**] This work was funded by the DFG IRTG 1422. D.M.E. thanks the Fonds der Chemischen Industrie for a PhD scholarship. We thank Prof. Dr. U. Diederichsen and Prof. Dr. M. Bennati for access to their spectrometers.

Supporting information for this article is available on the WWW under http://dx.doi.org/10.1002/anie.201307594.

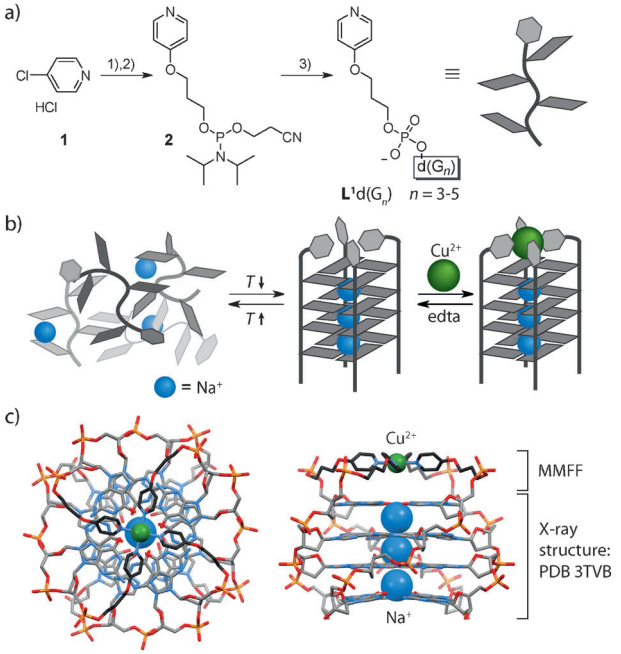

Figure 1. a) Synthesis of 5′-ligand-functionalized guanine-rich oligonucleotides $\mathbf{L^1}d(G_n)$ with $n = 3$–5. Reaction conditions: 1) 1,3-propanediol, NaOH, DMSO, 100 °C overnight; 2) $P(OCH_2CH_2CN)(NiPr_2)Cl$, *N*,*N*-diisopropylethylamine, THF, RT, 1 h; 3) automated solid-state DNA synthesis. b) Self-assembly of G-quadruplex $[\mathbf{L^1}d(G_4)]_4$ from single strands, incorporation of Cu^{II} ions, and removal of Cu^{II} with H_2EDTA^{2-} (edta). c) Molecular model of $Cu^{II}[\mathbf{L^1}d(G_4)]_4$ in top (left) and side (right) views; see the Supporting Information for details.

(ca. 4 d at 4 °C to reach equilibrium at a DNA concentration of 7 μM), so all samples were subjected to a previously reported freeze–thaw process which greatly increased the quadruplex formation rate.[26] Tetramolecular quadruplexes are known to prefer a parallel orientation (all strands aligned with the same 3′–5′ polarity) which is an essential requirement for the realization of the desired metal-chelating system.[25]

The hybridization of $\mathbf{L^1}d(G_4)$ was monitored by CD spectroscopy. A parallel G-quadruplex typically gives rise to a characteristic spectrum with a positive band at around 260 nm and a negative one at 240 nm, which indeed was observed for the ligand-modified G-quadruplex $[\mathbf{L^1}d(G_4)]_4$ (Figure 2a).[27] Additional support for the quadruplex formation came from the observation of a hyperchromic shift of the absorbance at 295 nm.[28] As described previously, thermal difference spectra of the single strand and quadruplex were also used to identify the quadruplex formation unequivocally (see the Supporting Information for details).[29] The decrease in absorbance at 295 nm upon denaturation was used to determine the nonequilibrium melting temperatures $T_{1/2}$ of the different quadruplex assemblies as a measure for their relative thermodynamic stabilities.

Subsequently, various transition-metal ions were added. The addition of Ni^{II} ions to the quadruplex $[\mathbf{L^1}d(G_4)]_4$ leads to a melting temperature increase of $\Delta T_{1/2} = 15$ °C. Surprisingly, this effect is even more pronounced for Cu^{II} ions with a remarkable increase of $\Delta T_{1/2} = 20$ °C (Figure 2b). It is interesting to compare this observation with a recent report

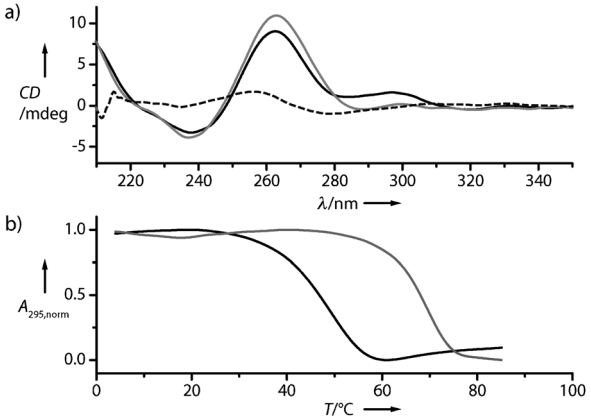

Figure 2. a) CD spectra of $[\mathbf{L^1}d(G_4)]_4$ in the absence (black curve) and presence (gray curve) of Cu^{II} at 4 °C and after melting at 85 °C (dotted line); b) UV/Vis thermal denaturation curves of $[\mathbf{L^1}d(G_4)]_4$ in the absence (black line) and presence of Cu^{II} (gray line). Absorbance is measured at 295 nm and normalized. Conditions: 7 μM $\mathbf{L^1}d(G_4)$, 10 mM sodium cacodylate, 100 mM NaCl, 0 or 7 μM $CuSO_4$.

describing the destabilization of unmodified quadruplexes by the presence of excess Cu^{II}.[30] The stoichiometry of Cu^{II} ions binding to the quadruplex was estimated to be 1:1 for $Cu^{II}/[\mathbf{L^1}d(G_4)]_4$ as determined by the changes in the UV/Vis spectrum (Figure 3a). The molecular model (Figure 1c and the Supporting Information) suggests a square-planar arrangement of the four pyridine arms around the Cu^{II} center.

In contrast, we found that the addition of Ag^I ions causes a destabilization with $\Delta T_{1/2} = -16$ °C, which is in good agree-

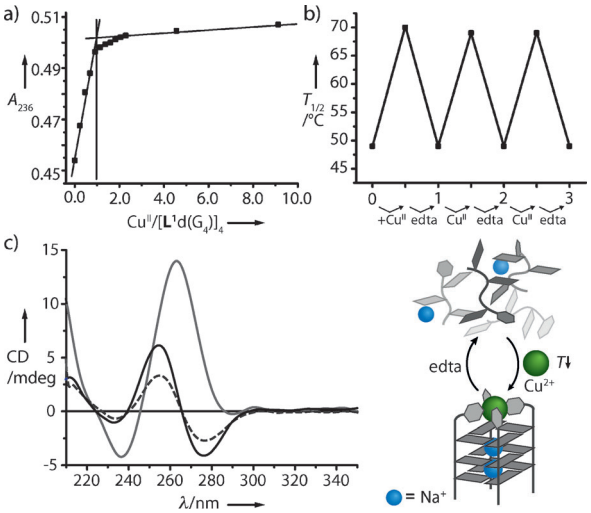

Figure 3. a) UV/Vis absorbance titration measured at 236 nm upon addition of Cu^{II} ions to $[\mathbf{L^1}d(G_4)]_4$ at 4 °C. The vertical line denotes the approximate binding stoichiometry of 1:1 $Cu^{II}/[\mathbf{L^1}d(G_4)]_4$; b) Melting temperature cycle for the recurring stabilization and destabilization of the G-quadruplex $[\mathbf{L^1}d(G_4)]_4$ by the alternate addition of Cu^{II} and edta (7 μM $\mathbf{L^1}d(G_4)$, 10 mM sodium cacodylate, 100 mM NaCl, $CuSO_4$ and edta additions in 1 equiv steps); c) Left: CD spectra of $[\mathbf{L^1}d(G_3)]_4$ (15 μM $\mathbf{L^1}d(G_3)$, 10 mM sodium cacodylate, 100 mM NaCl, 0 or 7 μM $CuSO_4$) in the presence (gray line) and absence of Cu^{II} at 4 °C (black) and after melting at 35 °C (dotted line); Right: self-assembly of $Cu^{II}[\mathbf{L^1}d(G_3)]_4$ and denaturation upon edta addition. No quadruplex formation is observed in the absence of Cu^{II}.

ment with the reported behavior for unmodified G-quadruplexes.[31] These findings indicate a different mode of interaction for the usually linear-coordinated Ag^{I} ions than for Cu^{II} or Ni^{II} ions, which prefer a square-planar or axially distorted octahedral coordination environment when they are offered four pyridine ligands.

To further support the binding of the Cu^{II} and Ni^{II} ions to the $(pyridine)_4$ motif, control strands $\mathbf{L}^{1*}d(G_n)$ were synthesized, in which the pyridyl ligand was replaced by a phenyl group lacking the donor functionality (see the Supporting Information). In the absence of transition-metal cations, the corresponding quadruplexes showed higher thermal stability than those with the pyridyl units, which might be explained by the more favorable π–π stacking of the electron-rich phenyl rings to the 5′-guanine tetrad in $[\mathbf{L}^{1*}d(G_4)]_4$, as well as the less favorable solubilization of the apolar phenyl groups in the aqueous buffer. Treatment of the control quadruplexes $[\mathbf{L}^{1*}d(G_4)]_4$ with Ni^{II} or Cu^{II} ions did not lead to any changes in stability; for Ag^{I}, however, a decrease in stability was detected, similar to that found with $[\mathbf{L}^{1}d(G_4)]_4$ ($\Delta T_{1/2} = -15\,^{\circ}C$). These results are in accordance with the tetracoordination of Ni^{II} and Cu^{II} to the pyridyl donors in $[\mathbf{L}^{1}d(G_4)]_4$ leading to a highly stabilizing square-planar (or, with two further apical ligands, an axially distorted octahedral) complex, whereas the predominant binding mode of Ag^{I} seems to be independent of the presence of the pyridine units.

The high stability of the Cu^{II}-G-quadruplex can be reversed by removal of the Cu^{II} ions with ethylenediaminetetraacetic acid (edta) as a chelating agent, which leads to the complete regeneration of the melting behavior corresponding to the metal-free G-quadruplex $[\mathbf{L}^{1}d(G_4)]_4$ (see the Supporting Information). This cycle of stabilization and destabilization can be repeated several times, demonstrating the reversibility of the metal–quadruplex assembly (Figure 3b).

To further investigate the effect of the metal complexation, oligonucleotide strands with guanine sequences of different lengths were synthesized. The longer quadruplex $[\mathbf{L}^{1}d(G_5)]_4$ exhibits an increase in melting temperature of $\Delta T_{1/2} = 40\,^{\circ}C$ relative to $[\mathbf{L}^{1}d(G_4)]_4$. As observed for $[\mathbf{L}^{1}d(G_4)]_4$, addition of Cu^{II} to $[\mathbf{L}^{1}d(G_5)]_4$ stabilizes the G-quadruplex, whereas addition of Ag^{I} leads to a destabilization (Figure S20).

In contrast, a shorter guanine sequence of $n = 3$ does not lead to G-quadruplex formation, even at 4 °C, indicating a melting temperature below 4 °C, which corresponds to a decrease of more than 45 °C relative to the melting temperature of $[\mathbf{L}^{1}d(G_4)]_4$. G-quadruplex formation can be triggered, however, by addition of Cu^{II} ions prior to annealing. These results are confirmed by the CD spectra, which show no typical quadruplex bands in the absence of Cu^{II} ions. Upon addition of Cu^{II} ions the formation of a quadruplex structure can be observed unambiguously (Figure 3c). Subsequent addition of edta at 4 °C leads to the rapid denaturation of this quadruplex (Figure S26).

In order to confirm these UV and CD spectroscopic results and to evaluate the presence of higher order structures like G-wires, the quadruplex formation was monitored by polyacrylamide gel electrophoresis (PAGE), as the migration length of the G-quadruplexes should be clearly distinguishable from that of single strands or higher-order aggregates. UV-shadowing and the G-quadruplex-sensitive fluorescent dye protoporphyrin IX (PPIX) were used to visualize the bands.[32] Indeed the PPIX-stained gel shows fluorescence in lanes 4–6 and 8, thus indicating the presence of intact G-quadruplexes (Figure 4). Compared to the reference DNA

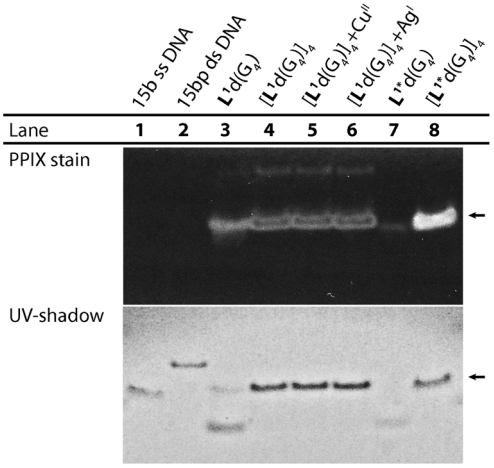

Figure 4. Nondenaturing gel electrophoresis of $[\mathbf{L}^{1}d(G_4)]_4$ and control strand $[\mathbf{L}^{1*}d(G_4)]_4$. G-quadruplex bands were first visualized by staining the gel with PPIX (upper picture) and then by UV-shadowing (lower picture). The arrows denote the same migration length in the gels. See the Supporting Information for details.

samples, the migration lengths correspond to those of discrete G-quadruplexes. No fluorescence is visible in the single- and double-stranded controls (lanes 1 and 2). The fluorescence in lanes 3 and 7 can be attributed to partial G-quadruplex formation during the PAGE experiment. No differences between the samples containing only the G-quadruplex (lane 4) and those with additional Cu^{II} (lane 5) or Ag^{I} (lane 6) are observed, indicating the preservation of the G-quadruplex assemblies.

To gain further insight into the coordination environment, EPR measurements were performed on a frozen solution of the $Cu^{II}[\mathbf{L}^{1}d(G_4)]_4$ quadruplex. The Cu^{II}-bound G-quadruplex shows a signal centered at around 300 mT typical of a mononuclear Cu^{II} complex. The absence of a resonance at half-field (ca. 160 mT) in the EPR spectra recorded in the temperature range 10–70 K, characteristic of a $\Delta M_S = \pm 2$ transition, indicates that there are no other Cu^{II} species of higher nuclearity (Figure S30).

As depicted in Figure 5, the EPR spectrum (black line) shows the hyperfine structure from one copper ($I_{Cu} = 3/2$) atom and superhyperfine structure from nitrogen ($I_N = 1$) atoms. The EPR spectrum was simulated using slightly rhombic $\boldsymbol{g}$ and $\boldsymbol{A}^{Cu}$ tensors. Although the $g_{x,y}$ region is particularly complex, since the Cu and ^{14}N hyperfine coupling are of similar magnitude, the spectrum can be well simulated considering a CuN_4 unit (Figure 5, gray line; simulation parameters are given in the legend). The parameter R, defined as $R = (g_2 - g_1)/(g_3 - g_2)$, can be indicative of the ground state of the copper(II) ion.[33] For the Cu^{II} quadruplex,

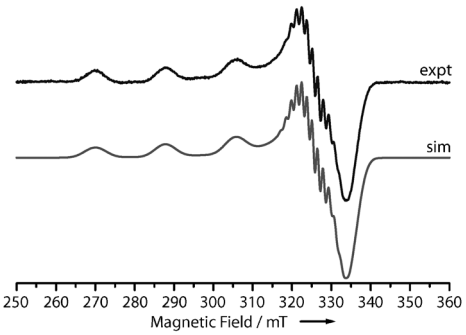

Figure 5. X-band continuous-wave (CW) EPR spectrum of a frozen solution of $Cu^{II}[\mathbf{L}^1d(G_4)]_4$ (sodium cacodylate 10 mM, NaCl 100 mM, $\mathbf{L}^1d(G_4)$ 615 μM, $CuSO_4$ 152 μM, 10 vol% glycerol) and simulation (shown in gray). Experimental parameters: 9.4 GHz, $T = 50$ K, microwave power: 0.6325 mW, conversion time: 123 ms, modulation amplitude: 10 G, modulation frequency: 100 kHz, 1 h signal averaging. The spectrum was simulated using Matlab-based toolbox Easyspin (version 4.51).[34] Simulation parameters are: $g_{x,y,z} = 2.0470, 2.0687, 2.2635$; $A(Cu) = [47\ 45\ 552]$ MHz; $A(N) = [40\ 39\ 40]$ MHz; linewidth = 5 G.

a value of $R = 0.11$ was found, which indicates that the greater contribution to the ground state arises from a $d_{x^2-y^2}$ orbital, consistent for copper coordinated in a square-planar, square-pyramidal, or distorted-octahedral environment. In order to confirm the UV/Vis and CD spectroscopic results on the reversibility of the metal incorporation, the Cu^{II}–G-quadruplex was treated with edta, thus giving the typical EPR spectrum of the Cu^{II}–edta complex (Figure S31).

In conclusion, we have synthesized and characterized novel G-quadruplexes composed of four parallel-aligned guanine sequences carrying pyridine ligands at their 5′-ends. As a result, four pyridine donors are prearranged in the fashion of a chelate ligand and thus show a high affinity for the square-planar coordination of the transition-metal cations Cu^{II} and Ni^{II}. Furthermore, the addition of Cu^{II} or Ni^{II} ions substantially stabilizes the quadruplexes $[\mathbf{L}^1d(G_n)]_4$ ($n = 3$–5) towards thermal denaturation as was shown in melting experiments based on UV/Vis and CD spectroscopy.

Our current efforts are devoted to the development of a ligand-modified nucleoside that can be incorporated in internal sequence positions, thus making it possible to synthesize metal-stabilized monomolecular quadruplexes whose folding topology and loop composition may be systematically varied. Libraries of such metal-carrying quadruplexes acting as spectroscopically traceable probes will then be used in the search for new oligonucleotide–protein interactions. The incorporation of further transition-metal complexes in the 3′ and internal positions will enable us to study metal–metal interactions.[16] We see potential applications of such metallated G-quadruplexes in the fields of structural bionanotechnology, molecular electronics, magnetism, and catalysis.[35]

Received: August 28, 2013
Published online: November 7, 2013

Keywords: bioinorganic chemistry · DNA · G-quadruplexes · metal–base pair · supramolecular chemistry

[1] J. Choi, T. Majima, *Chem. Soc. Rev.* **2011**, *40*, 5893 – 5909.
[2] a) S. Burge, G. N. Parkinson, P. Hazel, A. K. Todd, S. Neidle, *Nucleic Acids Res.* **2006**, *34*, 5402 – 5415; b) N. W. Luedtke, *Chimia* **2009**, *63*, 134 – 139; c) L. Davis, N. Maizels, *EMBO J.* **2011**, *30*, 3878 – 3879.
[3] a) C. Schaffitzel, I. Berger, J. Postberg, J. Hanes, H. J. Lipps, A. Pluckthun, *Proc. Natl. Acad. Sci. USA* **2001**, *98*, 8572 – 8577; b) G. Biffi, D. Tannahill, J. McCafferty, S. Balasubramanian, *Nat. Chem.* **2013**, *5*, 182 – 186; c) E. Y. N. Lam, D. Beraldi, D. Tannahill, S. Balasubramanian, *Nat. Commun.* **2013**, *4*, 1796.
[4] a) J. T. Davis, *Angew. Chem.* **2004**, *116*, 684 – 716; *Angew. Chem. Int. Ed.* **2004**, *43*, 668 – 698; b) S. Neidle, *FEBS J.* **2010**, *277*, 1118 – 1125; c) T. A. Brooks, L. H. Hurley, *Genes Cancer* **2010**, *1*, 641 – 649; d) G. W. Collie, G. N. Parkinson, *Chem. Soc. Rev.* **2011**, *40*, 5867 – 5892; e) S. Balasubramanian, L. H. Hurley, S. Neidle, *Nat. Rev. Drug Discovery* **2011**, *10*, 261 – 275.
[5] A. N. Lane, J. B. Chaires, R. D. Gray, J. O. Trent, *Nucleic Acids Res.* **2008**, *36*, 5482 – 5515.
[6] A. Nadler, J. Strohmeier, U. Diederichsen, *Angew. Chem.* **2011**, *123*, 5504 – 5508; *Angew. Chem. Int. Ed.* **2011**, *50*, 5392 – 5396.
[7] C. Sissi, B. Gatto, M. Palumbo, *Biochimie* **2011**, *93*, 1219 – 1230.
[8] a) M. A. Keniry, *Biopolymers* **2000**, *56*, 123 – 146; b) T. Simonsson, *Biol. Chem.* **2001**, *382*, 621 – 628; c) X. Cang, J. Šponer, I. E. Cheatham, *J. Am. Chem. Soc.* **2011**, *133*, 14270 – 14279.
[9] For recent examples see the issue of *Chem. Soc. Rev.* dedicated to the theme "Advances in DNA-based nanotechnology: E. Stulz, G. H. Clever, M. Shionoya, C. Mao, *Chem. Soc. Rev.* **2011**, *40*, 5633 – 5635.
[10] a) N. Rosi, C. Mirkin, *Chem. Rev.* **2005**, *105*, 1547 – 1562; b) N. C. Seeman, *Annu. Rev. Biochem.* **2010**, *79*, 65 – 87; c) E. Stulz, *Chem. Eur. J.* **2012**, *18*, 4456 – 4469.
[11] a) S. N. Georgiades, N. H. Abd Karim, K. Suntharalingam, R. Vilar, *Angew. Chem.* **2010**, *122*, 4114 – 4128; *Angew. Chem. Int. Ed.* **2010**, *49*, 4020 – 4034; b) O. Doluca, J. M. Withers, V. V. Filichev, *Chem. Rev.* **2013**, *113*, 3044 – 3083.
[12] a) G. H. Clever, C. Kaul, T. Carell, *Angew. Chem.* **2007**, *119*, 6340 – 6350; *Angew. Chem. Int. Ed.* **2007**, *46*, 6226 – 6236; b) J. Müller, *Eur. J. Inorg. Chem.* **2008**, 3749 – 3763; c) G. H. Clever, M. Shionoya, *Coord. Chem. Rev.* **2010**, *254*, 2391 – 2402; d) Y. Takezawa, M. Shionoya, *Acc. Chem. Res.* **2012**, *45*, 2066 – 2076; e) P. Scharf, J. Müller, *ChemPlusChem* **2013**, *78*, 20 – 34; For transition metal binding nucleobase-quartets see: f) K. Uchida, A. Toyama, Y. Tamura, M. Sugimura, F. Mitsumori, Y. Furukawa, H. Takeuchi, I. Harada, *Inorg. Chem.* **1989**, *28*, 2067 – 2073; g) M. Roitzsch, B. Lippert, *Angew. Chem.* **2006**, *118*, 153 – 156; *Angew. Chem. Int. Ed.* **2006**, *45*, 147 – 150.
[13] For other pyridine-based metal–base pairs see: a) E. Meggers, P. L. Holland, W. B. Tolman, F. E. Romesberg, P. G. Schultz, *J. Am. Chem. Soc.* **2000**, *122*, 10714 – 10715; b) K. Tanaka, Y. Yamada, M. Shionoya, *J. Am. Chem. Soc.* **2002**, *124*, 8802 – 8803.
[14] D. Böhme, N. Düpre, D. A. Megger, J. Müller, *Inorg. Chem.* **2007**, *46*, 10114 – 10119.
[15] R. Freeman, T. Finder, I. Willner, *Angew. Chem.* **2009**, *121*, 7958 – 7961; *Angew. Chem. Int. Ed.* **2009**, *48*, 7818 – 7821.
[16] a) K. Tanaka, A. Tengeiji, T. Kato, N. Toyama, M. Shionoya, *Science* **2003**, *299*, 1212 – 1213; b) S. S. Mallajosyula, S. K. Pati, *Angew. Chem.* **2009**, *121*, 5077 – 5081; *Angew. Chem. Int. Ed.* **2009**, *48*, 4977 – 4981; c) G. H. Clever, S. J. Reitmeier, T. Carell, O. Schiemann, *Angew. Chem.* **2010**, *122*, 5047 – 5049; *Angew. Chem. Int. Ed.* **2010**, *49*, 4927 – 4929; d) T. Ehrenschwender, W. Schmucker, C. Wellner, T. Augenstein, P. Carl, J. Harmer, F. Breher, H.-A. Wagenknecht, *Chem. Eur. J.* **2013**, *19*, 12547 – 12552.

[17] K. Tanaka, G. H. Clever, Y. Takezawa, Y. Yamada, C. Kaul, M. Shionoya, T. Carell, *Nat. Nanotechnol.* **2006**, *1*, 190 – 194.
[18] S. Liu, G. H. Clever, Y. Takezawa, M. Kaneko, K. Tanaka, X. Guo, M. Shionoya, *Angew. Chem.* **2011**, *123*, 9048 – 9052; *Angew. Chem. Int. Ed.* **2011**, *50*, 8886 – 8890.
[19] Y. Takezawa, W. Maeda, K. Tanaka, M. Shionoya, *Angew. Chem.* **2009**, *121*, 1101 – 1104; *Angew. Chem. Int. Ed.* **2009**, *48*, 1081 – 1084.
[20] J.-L. H. A. Duprey, Y. Takezawa, M. Shionoya, *Angew. Chem.* **2013**, *125*, 1250 – 1254; *Angew. Chem. Int. Ed.* **2013**, *52*, 1212 – 1216.
[21] For examples of metal-mediated control over the tertiary structure of DNA architectures see: a) J. S. Choi, C. W. Kang, K. Jung, J. W. Yang, Y.-G. Kim, H. Han, *J. Am. Chem. Soc.* **2004**, *126*, 8606 – 8607; b) H. Yang, H. F. Sleiman, *Angew. Chem.* **2008**, *120*, 2477 – 2480; *Angew. Chem. Int. Ed.* **2008**, *47*, 2443 – 2446; c) N. Düpre, L. Welte, J. Gómez-Herrero, F. Zamora, J. Müller, *Inorg. Chim. Acta* **2009**, *362*, 985 – 992; d) J. R. Burns, J. Zekonyte, G. Siligardi, R. Hussain, E. Stulz, *Molecules* **2011**, *16*, 4912 – 4922.
[22] N. M. Smith, S. Amrane, F. Rosu, V. Gabelica, J.-L. Mergny, *Chem. Commun.* **2012**, *48*, 11464 – 11466.
[23] Y. Xu, Y. Suzuki, T. Lonnberg, M. Komiyama, *J. Am. Chem. Soc.* **2009**, *131*, 2871 – 2874.
[24] D. Miyoshi, H. Karimata, Z.-M. Wang, K. Koumoto, N. Sugimoto, *J. Am. Chem. Soc.* **2007**, *129*, 5919 – 5925.
[25] J.-L. Mergny, A. de Cian, A. Ghelab, B. Saccà, L. Lacroix, *Nucleic Acids Res.* **2005**, *33*, 81 – 94.
[26] Q. Zhai, M. Deng, L. Xu, X. Zhang, X. Zhou, *Bioorg. Med. Chem. Lett.* **2012**, *22*, 1142 – 1145.
[27] a) P. Balagurumoorthy, S. K. Brahmachari, D. Mohanty, M. Bansal, V. Sasisekharan, *Nucleic Acids Res.* **1992**, *20*, 4061 – 4067; b) S. Masiero, R. Trotta, S. Pieraccini, S. de Tito, R. Perone, A. Randazzo, G. P. Spada, *Org. Biomol. Chem.* **2010**, *8*, 2683 – 2692.
[28] J.-L. Mergny, A.-T. Phan, L. Lacroix, *FEBS Lett.* **1998**, *435*, 74 – 78.
[29] J.-L. Mergny, J. Li, L. Lacroix, S. Amrane, J. B. Chaires, *Nucleic Acids Res.* **2005**, *33*, e138.
[30] D. Monchaud, P. Yang, L. Lacroix, M.-P. Teulade-Fichou, J.-L. Mergny, *Angew. Chem.* **2008**, *120*, 4936 – 4939; *Angew. Chem. Int. Ed.* **2008**, *47*, 4858 – 4861.
[31] a) R. M. Izatt, J. J. Christensen, J. H. Rytting, *Chem. Rev.* **1971**, *71*, 439 – 481; b) X.-H. Zhou, D.-M. Kong, H.-X. Shen, *Anal. Chem.* **2010**, *82*, 789 – 793.
[32] a) T. Li, E. Wang, S. Dong, *Anal. Chem.* **2010**, *82*, 7576 – 7580; b) D.-L. Ma, H.-Z. He, K.-H. Leung, H.-J. Zhong, D. S.-H. Chan, C.-H. Leung, *Chem. Soc. Rev.* **2013**, *42*, 3427 – 3440.
[33] B. J. Hathaway, D. E. Billing, *Coord. Chem. Rev.* **1970**, *5*, 143 – 207.
[34] S. Stoll, A. Schweiger, *J. Magn. Reson.* **2006**, *178*, 42 – 55.
[35] M. Wilking, U. Hennecke, *Org. Biomol. Chem.* **2013**, *11*, 6940 – 6945.

